JACS
JOURNAL OF THE AMERICAN CHEMICAL SOCIETY
Article
pubs.acs.org/JACS

Micelle Structure and Hydrophobic Hydration

Joshua A. Long, Blake M. Rankin, and Dor Ben-Amotz*

Department of Chemistry, Purdue University, West Lafayette, Indiana 47907, United States

Supporting Information

ABSTRACT: Despite the ubiquity and utility of micelles self-assembled from aqueous surfactants, longstanding questions remain regarding their surface structure and interior hydration. Here we combine Raman spectroscopy with multivariate curve resolution (Raman-MCR) to probe the hydrophobic hydration of surfactants with various aliphatic chain lengths, and either anionic (carboxylate) or cationic (trimethylammonium) head groups, both below and above the critical micelle concentration. Our results reveal significant penetration of water into micelle interiors, well beyond the first few carbons adjacent to the headgroup. Moreover, the vibrational C-D frequency shifts of solubilized deuterated *n*-hexane confirm that it resides in a dry, oil-like environment (while the localization of solubilized benzene is sensitive to headgroup charge). Our findings imply that the hydrophobic core of a micelle is surrounded by a highly corrugated surface containing hydrated non-polar cavities whose depth increases with increasing surfactant chain length, thus bearing a greater resemblance to soluble proteins than previously recognized.

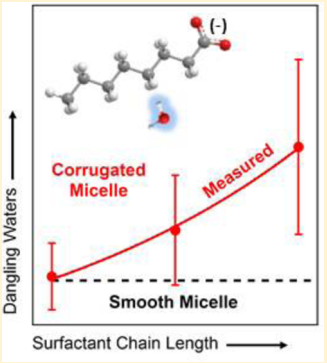

INTRODUCTION

Micelles formed of surfactants dissolved in water are ubiquitous, not only as household soaps and detergents but also in drug delivery, oil recovery, and environmental remediation applications. Although micelles are often envisioned as spherical aggregates with a dry hydrocarbon core and a water-exposed polar exterior,[1−6] longstanding questions remain regarding the surface roughness and hydrophobic hydration of micelles.[7−16] Here we address these questions by combining Raman spectroscopy and multivariate curve resolution (Raman-MCR)[17−20] to reveal that micelles contain hydrated non-polar cavities whose water-exposed surface area increases with surfactant chain length.

Previous NMR,[7,10,21] neutron scattering,[22−24] X-ray scattering,[8,13] EPR,[25] and molecular dynamics (MD) simulations,[24,26−29] have led to widely varying conclusions regarding micelle structure and hydration.[1−13] Although it is often stated that water penetration does not extend significantly beyond the first 2−4 methylene groups adjacent to the surfactant headgroup,[22−25] numerous early NMR,[7,10] X-ray,[8] thermodynamic[30−32] and transport[32,33] property studies concluded that micelles have highly hydrated and/or nonspherical structures with up to ∼10 water molecules per surfactant, and up to ∼50% of the total volume of a micelle consisting of water (although in some of these studies the inferred hydration includes water molecules bound to the polar head groups).

Figure 1 compares predictions and structures pertaining to several micelle models. The surface area predictions in Figure 1A were obtained assuming an idealized spherical micelle structure composed of surfactants of various carbon chain lengths with a uniform liquid-like density and experimentally derived aggregation numbers (see Supporting Information for further details). Importantly, these predictions imply that such idealized smooth spherical micelles would have an approximately chain-length independent surface area per surfactant. They also predict that about 60% of the surface of such micelles is non-polar, implying that over 20% of the surfactant non-polar groups are exposed to water. Although these predictions pertain to a minimalist spherical model, they are generally consistent with predictions obtained using more sophisticated spherical statistical mean field micelle models[2,4,5,12] such as the Gruen model illustrated in Figure 1B,[34] which predicts that "...all segments of the chain spend some time in a hydrophilic environment...", although segments near the headgroup are exposed to water 80%−90% of the time, compared to 10%−20% for segments far from the headgroup.[4,5] Figure 1C shows a cross-sectional snapshot of a decyltrimethylammonium bromide (C_{10}TAB) micelle derived from neutron scattering measurements combined with EPSR MD simulations.[24] The latter study concluded that "surfactant tail groups are hidden away from the solvent to form a central dry hydrophobic core...", although there are a "...significant number of alkyl groups in the polar shell of the micelle". In contrast, Figure 1D[35] illustrates a quite different micelle structure inferred from small-angle X-ray scattering measurements of aqueous sodium octanoate (C_7COONa) surfactant solutions, implying that micelles have a quite small hydrophobic core with "considerable hydration of the micelles and penetration of water between the hydrocarbon chains". The latter conclusion is generally consistent with the Menger model, which implies that "although micelles have a non-polar core, water penetrates deeply into the structure".[10]

Here, we use Raman-MCR[17−20,36−39] to critically test and distinguish such alternative micelle structures, by probing the hydration shells of C_nCOONa and C_nTAB surfactants of

Received: July 2, 2015
Published: July 29, 2015

DOI: 10.1021/jacs.5b06655
J. Am. Chem. Soc. 2015, 137, 10809−10815

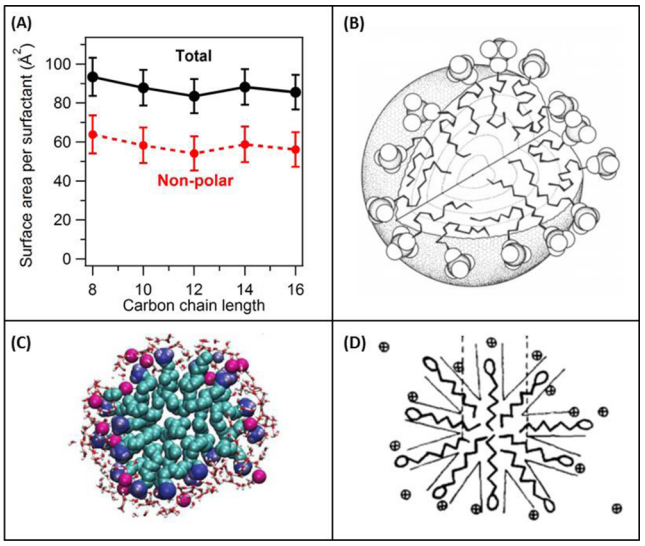

Figure 1. (A) Water-exposed surface area of an idealized spherical micelle (with a liquid like density). About 60% of the surface is predicted to be non-polar, with an approximately chain-length-independent surface area per surfactant. The error bars arise from uncertainties in the experimentally derived aggregation numbers (as reported in Supporting Information). (B) Schematic of the Gruen micelle model obtained using statistical mean field calculations, assuming a liquid-like density with a dry core.[34] (C) Cross-section of a micelle obtained from neutron scattering measurements and EPSR MD simulations.[24] (D) Schematic micelle model inferred from X-ray scattering measurements,[35] showing deep "wedges" into which water can penetrate, surrounding a small dry core.

various chain lengths ($7 \leq n \leq 12$), at concentrations ranging from ~0.5 times below to ~10 times above the critical micelle concentration (CMC), as well as after solubilizing *n*-hexane-d_{14} and benzene-d_6. Of the micelle structures illustrated in Figure 1, our experimental findings are most consistent with that shown in Figure 1D,[35] as well as with the Menger model.[10]

The remainder of this manuscript is organized as follows. The Results section is divided into four subsections. The first two subsections describe our Raman-MCR findings pertaining to aqueous C_nCOONa and C_nTAB surfactants (including the procedures we used to highlight vibrational features arising from water molecules adjacent to the surfactant hydrocarbon C_n tails); the third subsection describes our observations of water dangling OH features, whose surfactant chain-length dependence provides critical evidence regarding micelle structure; and the fourth subsection describes how we used *n*-hexane and benzene solubilization to probe the core polarity of C_nCOONa and C_nTAB micelles. Finally, the Summary and Discussion section provides an overview of our conclusions and possible biochemical implications.

RESULTS

Anionic Surfactants. Figure 2A shows the Raman spectra of pure water and a 0.05 M aqueous solution of sodium decanoate (C_9COONa), as well as the resulting surfactant solute-correlated (SC) spectrum obtained using Raman-MCR. More specifically, the latter SC spectrum of C_9COONa was obtained by using self-modeling curve resolution (SMCR) to decompose the measured Raman spectra of aqueous surfactant solutions into bulk solvent (pure water) and SC components.[17,18,36,38] The resulting SC spectrum, purple curve in Figure 2A, reveals Raman features arising from the intra-

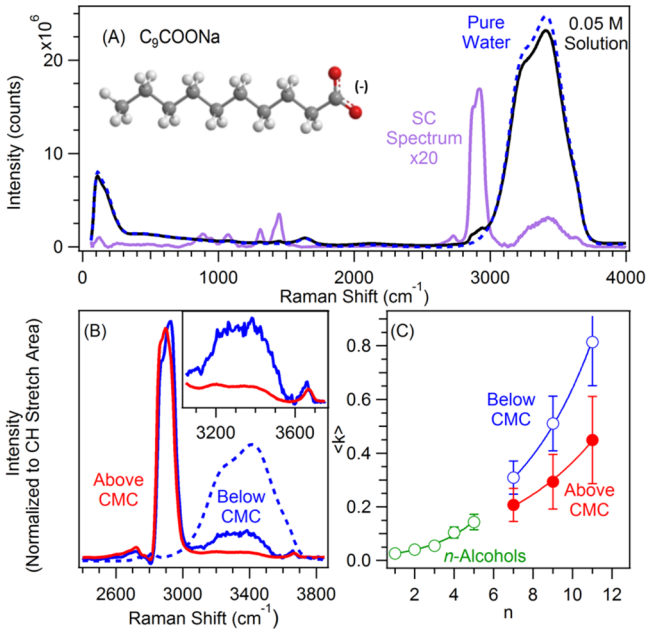

Figure 2. (A) Raman spectra of pure water (dashed blue), an aqueous solution of 0.05 M sodium decanoate (C_9COONa) (black), and the resulting SC spectrum of 0.05 M C_9COONa (purple) after subtracting a linear baseline. (B) SC spectra of C_9COONa with sodium formate headgroup subtraction below the CMC (0.05 M, solid blue) and above the CMC (1.0 M, red). The inset in (B) shows an expanded view of the hydration shell OH bands. (C) The average number of excess dangling OH groups per hydration shell $\langle k \rangle$ for *n*-alcohols and C_nCOONa surfactants at concentrations below (open blue points) and 5 times above their respective CMCs (solid red points).

molecular vibrations of the surfactant, such as the surfactant CH stretch (at ~2800−3050 cm^{-1}), as well as hydration shell OH stretching features (at ~3100−3700 cm^{-1}), arising from water molecules whose vibrational structure is perturbed by the surfactant. Note that previous studies indicate that Na^+ has little or no influence on Raman-MCR spectra (as the OH stretch vibration of water around Na^+ closely resembles the OH stretch of bulk water molecules),[40] and therefore the SC OH stretch band arises primarily from the hydration shell of the anionic surfactant. The broad OH features at ~3400 cm^{-1} is due largely to water molecules that are H-bonded to the carboxylate headgroup of C_9COONa, as evidenced by the appearance of a very similar band in the hydration shell spectrum of sodium formate (HCOONa).[20]

In order to suppress the SC OH band arising from the carboxylate headgroup hydration shell, and thus highlight features arising from the hydrophobic hydration shell of the surfactant's tail (C_9), we have implemented a Raman-MCR headgroup subtraction procedure by including an equimolar concentration of HCOONa in the solvent reference solution, as previously described.[20] In other words, since the carboxylate headgroup is now present in both the surfactant solution and in the solvent reference solution, the resulting Raman-MCR SC spectrum contains OH features arising primarily from the surfactant's hydrophobic hydration shell. Figure 2B shows headgroup-subtracted SC spectra obtained in this way, both below (0.05 M, blue) and above (1.0 M, red) the CMC of C_9COONa (~0.098 M).[41] Note that the formation of micelles induces changes in both the surfactant's hydration shell OH band and its tail CH (whose mean frequency is shifted by about ~8 cm^{-1}, and shape is changed, with little change in width).

DOI: 10.1021/jacs.5b06655
J. Am. Chem. Soc. 2015, 137, 10809−10815

The SC spectra in Figure 2B are normalized to the corresponding CH band area, and thus the associated SC OH bands (which are expanded in the inset panel) reveal the substantial decrease in the hydrophobic hydration shell OH population upon micelle formation.

The hydration shell OH bands shown in Figure 2B contain both broad H-bonded OH features between ~3100−3500 cm^{-1} and a relatively sharp peak at ~3660 cm^{-1}. The broad H-bonded OH band is quite similar to that previously observed in the hydrophobic hydration shells of alcohols,[18,19] and carboxylic acids,[20] whose highly polarized lower frequency shoulder at ~3200 cm^{-1} implies that water has greater tetrahedral order near non-polar groups (note that clathrate hydrates also contain a prominent polarized Raman band in this region).[18] The small sharp peak at ~3660 cm^{-1} arises from the excess population of dangling (non-H-bonded) OH groups on water molecules in non-polar hydration shells.[19,39] The fact that the dangling OH peak remains quite prominent after micelle formation implies that a substantial number of water molecules remain in contact with the surfactant tail (as further discussed below).

Although we are not able to precisely quantify the number of water molecules that remain in contact with the surfactant's non-polar tails in a micelle, the results in Figure 2B imply that those water molecules are more likely to contain dangling OH groups and thus less likely to be H-bonded. Moreover, the results in Figure 2B imply that between ~15% and ~60% of the water molecules that were in the non-polar surfactant hydration shell of an isolated (non-aggregated) surfactant remain after micelle formation. More specifically, these lower and upper bounds are obtained from the decrease in the H-bonded and dangling OH band areas upon micelle formation, respectively, (after correcting for the residual free monomer contribution). Note that the lower bound of ~15% is clearly an underestimate, as it is less than the value of ~20% predicted for idealized spherical micelle structures (as shown in Figure 1A). Moreover, our chain-length-dependent Raman-MCR results reveal that water penetrates significantly beyond the first few carbons near the polar headgroup, and provide strong evidence that micelles have a highly corrugated surface structure (as further explained in the Dangling OH Chain Length Dependence subsection), thus implying that more than 20% of the non-polar groups in a micelle are exposed to water.

Cationic Surfactants. Figure 3A shows the Raman spectra of pure water and a 0.05 M aqueous solution of decyltrimethylammonium bromide (C_{10}TAB), as well as the resulting surfactant Raman-MCR SC spectra (purple curve). The hydration shell OH band centered at ~3400 cm^{-1} in this case arises primarily from water molecules that are hydrogen bonded to the Br^- counterions, as evidenced by the fact that a similar band appears in the hydration shell spectrum of aqueous NaBr solutions.[40] In order to suppress the spectrum arising from water molecules H-bonded to Br^-, we used a counterion-subtraction procedure (analogous to the headgroup subtraction procedure), by adding NaBr to the solvent reference (with the same concentration as the surfactant solution), as previously described.[19,20] Figure 3B shows the SC spectra of C_{10}TAB obtained after implementing this counterion-subtraction procedure, both below (0.05 M) and above (1.0 M) CMC (~0.065 M).[41] Again, we observe aggregation-induced changes in both the hydration shell OH band, and the surfactant's CH band (whose mean frequency red-shifts by ~9 cm^{-1} upon micelle formation). However, the hydration shell of C_{10}TAB,

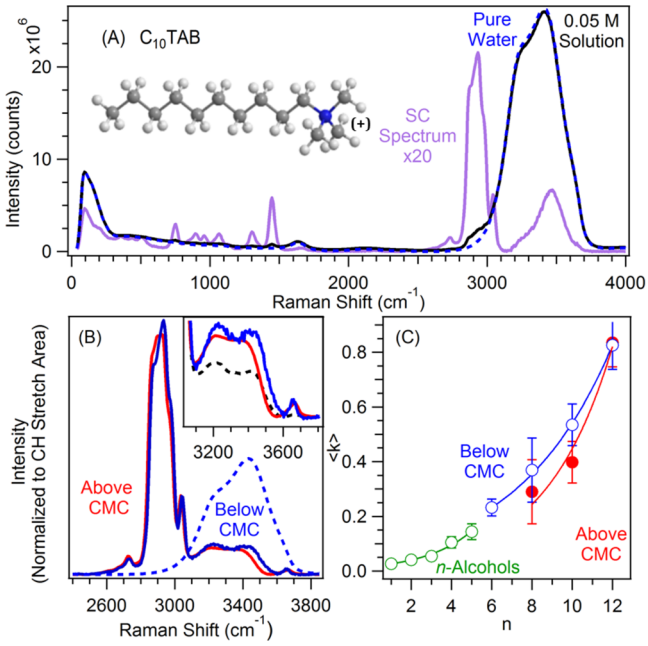

Figure 3. (A) Raman spectra of pure water (dashed blue) an aqueous solution of 0.05 M decyltrimethylammonium bromide (C_{10}TAB) (black), and the corresponding SC spectrum of 0.05 M C_{10}TAB (purple) after subtracting a linear baseline. (B) SC spectra of C_{10}TAB with Br^- counterion subtraction below the CMC (0.05 M, solid blue) and above (1.0 M, red) CMC. The inset in (B) compares the hydration shell spectra with counterion subtraction below and above CMC. The dashed black curve pertains to the hydration shell spectrum of a tetramethylammonium cation, scaled by a factor of 3/4 (since the cation contains four methyl groups while the surfactant headgroup contains three methyl groups). (C) The average number of excess dangling OH groups per hydration shell $\langle k \rangle$ for *n*-alcohols and C_nTAB surfactants, at concentrations below and 3 times above their respective CMCs.

and particularly the way it changes upon micelle formation, is quite different from that of the anionic (C_9COONa) surfactant. More specifically, upon micelle formation the C_{10}TAB hydration shell OH area only decreases by ~18 ± 2%, while its high-frequency edge is found to red-shift (by ~48 cm^{-1}). The small decrease in the SC OH band area is likely due to the fact that the trimethylammonium headgroup contributes significantly to the C_{10}TAB hydration shell spectrum, as evidenced by the headgroup OH band (dashed spectrum) in the inset panel of Figure 3B. The latter Raman-MCR headgroup SC OH was obtained from an equimolar solution of tetramethylammonium bromide, scaled by a factor of 3/4 (since the cation contains four methyl groups while the surfactant headgroup contains three methyl groups). Although the prominent headgroup contribution makes it difficult to quantify the number of H-bonded waters adjacent to the surfactant tail, it is clear that more than half of the H-bonded OH band area arises from water molecules around the headgroup. Moreover, the red-shift of the hydration shell OH band edge implies that the H-bonds between water molecules in the micelle are somewhat stronger than those in bulk water. More importantly, note that, once again, a prominent dangling OH peak at ~3660 cm^{-1} remains after micelle formation. Moreover, it is clear that those dangling OH groups arise from water molecules around the surfactant tail, as the headgroup OH spectrum in Figure 3B contains little evidence of a dangling

DOI: 10.1021/jacs.5b06655
J. Am. Chem. Soc. 2015, 137, 10809−10815

OH band.[19] Thus, the fact that the surfactant dangling OH peak remains prominent above CMC again implies that the surfactant hydrocarbon chains remain significantly hydrated in these cationic micelles (as further discussed in the following subsection).

Uncertainties regarding the $-N(CH_3)_3^+$ headgroup and Br^- counterion hydration make it difficult to quantify the C_nTAB SC micelle hydration shell band areas. This is in part because the $-N(CH_3)_3^+$ headgroup is rather hydrophobic and so is likely to partially dehydrate upon micelle formation.[42,43] Moreover, uncertainties regarding the degree of dehydration of the Br^- counterions further limit our ability to quantify micelle formation induced changes in the areas of H-bonded and dangling OH bands (as further described in the Supporting Information).

Dangling OH Chain Length Dependence. Figures 2C and 3C show how the excess number of dangling OH groups (per surfactant) $\langle k \rangle$ depends on surfactant chain length, both above (blue open points) and below (red solid points) CMC, as well as comparisons with previously reported $\langle k \rangle$ values obtained from aqueous *n*-alcohol solutions (green open points).[19] The $\langle k \rangle$ values were obtained from the area under the dangling OH peak in the SC spectrum, as previously described.[19] The solid points in Figures 2C and 3C represent the $\langle k \rangle$ values obtained after removing the contribution from free monomers that are in equilibrium with the micelles, assuming that the free monomer concentration is equal to the CMC (as further described in the Supporting Information). Comparisons of the open blue and green points in both Figures 2C and 3C indicate that the average number of surfactant dangling OH groups (before micelle formation) has a nonlinear chain length dependence that is roughly consistent with that previously reported for *n*-alcohols (and ascribed to the cooperativity of the dangling OH formation process).[19]

Comparisons of the open blue and solid red points in both Figures 2C and 3C imply that the excess number of dangling OH groups in the hydrophobic hydration shell of each surfactant in a micelle is comparable to that around a fully hydrated surfactant (below CMC). Most importantly, the number of such hydrophobic water molecules (per surfactant) clearly increases with chain length. The significance of this increase becomes evident when recalling that smooth spherical micelles are predicted to have an approximately chain-length independent non-polar surface area per surfactant, as indicated by the results in Figure 1A. Moreover, one would expect to see a chain-length independent dangling OH probability for nearly spherical micelles in which water only penetrates to the first 2–4 methylene groups adjacent to the polar headgroup (as is commonly assumed to be the case).[22−25] Thus, the fact that we have observed that $\langle k \rangle$ is strongly chain-length dependent implies that micelles do not have a nearly spherical (and smooth) structure, as water evidently remains in contact with the hydrocarbon chain well beyond the first 2–4 methylene groups adjacent to the headgroup. In other words, the fact that $\langle k \rangle$ increases with *n* above CMC implies that *micelle surfaces contain water-permeable cavities whose water-exposed surface area increases with increasing surfactant chain length*. Moreover, the results presented in the following subsections confirm that, underlying this highly corrugated and hydrophobically hydrated surface, there is dry oily core.

Uptake of Hydrophobic Probes by Micelles. Numerous previous studies have employed small molecules[13,44−50] or functionalized surfactants[7,10,21,51] to probe the hydration of micelle interiors. However, in many cases the probes have contained polar groups (such as −F, −Cl, or C═O)[7,10,46,50−52] which might carry water molecules into the micelle. Thus, we have chosen to probe the polarity of micelle interiors using non-polar perdeuterated *n*-hexane-d_{14} and benzene-d_6 probe molecules. Although we are not the first to employ benzene or alkanes as probes[44,45,47,48] of micelle interiors, these studies are the first to use Raman-MCR for such studies and (to the best of our knowledge) the first to use vibrational (C-D) frequency shifts to probe the polarity of micelle cores.

We have introduced the non-polar probes into micelles using a slow equilibration procedure,[53] rather than mechanical mixing or sonication (which might produce highly non-equilibrium structures). More specifically, we introduced the probes by placing a layer of oil (either *n*-hexane-d_{14} or benzene-d_6) over an aqueous surfactant solution (either C_9COONa or C_{10}TAB), as illustrated by the schematic in Figure 4A, and allowed the system to slowly equilibrate over a period of several days (or weeks). Raman spectra of the aqueous phase were collected periodically in order to quantify the uptake of the deuterated oil molecules by the non-deuterated micelles (as evidenced by the growing CD stretch bands in Figure 4).

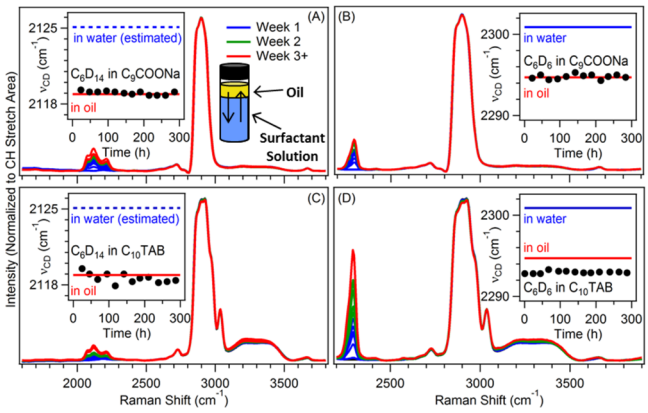

Figure 4. Surfactant SC spectra obtained 1 (blue), 2 (green), and 3 (red) weeks after the addition of deuterated hydrophobic probes into 1.0 M surfactant solutions. The schematic in panel A illustrates the oil/surfactant solution system. Addition of hexane-d_{14} (A) or benzene-d_6 (B) to C_9COONa micelles. Addition of hexane-d_{14} (C) or benzene-d_6 (D) to C_{10}TAB micelles. The inset panels display the frequency of the CD stretch Raman peak of the deuterated probe over time (black points) compared to the same deuterated probe in pure hexane (red line) or water (solid blue line for benzene-d_6 CD Raman peak in water, while the dotted blue line represents estimated hexane-d_{14} CD Raman peak position in water, obtained by assuming the same frequency difference as 1-hexanol-d_{13} from oil to water).

Figure 4 shows the resulting surfactant SC spectra obtained from 1.0 M aqueous solutions of C_9COONa (panels A and B) and C_{10}TAB (panels C and D) in the presence of hexane-d_{14} (panels A and C) and benzene-d_6 (panels B and D). In all cases, the intensity of the CD stretches of the micelle solubilized hexane-d_{14} (2120 cm^{-1}) and benzene-d_6 (2295 cm^{-1}) was found to slowly increase over time. Note that the low aqueous solubility of benzene (~0.023 M)[54] and much lower aqueous solubility of hexane (~1.1×10^{-4} M)[54] imply that the observed increase arises virtually entirely from uptake of these non-polar probe molecules by the micelles. Both molecules incorporated into the carboxylate micelles at similar rates, which was also similar to the rate at which hexane was taken up by the C_{10}TAB

DOI: 10.1021/jacs.5b06655
J. Am. Chem. Soc. 2015, 137, 10809−10815

micelles. However, benzene incorporated into the C_{10}TAB micelles at a somewhat higher rate (as further discussed below). After 3 weeks, the total number of solubilized probes was ~5 hexane-d_{14} molecules per C_{10}TAB micelle and ~8 per C_9COONa micelle, while ~11 benzene-d_6 molecules were taken up by each C_9COONa micelle and ~36 by each C_{10}TAB micelle. Since there are ~45 surfactants in both the C_9COONa and C_{10}TAB micelles,[55,56] our results indicate that each micelle contained significantly fewer probe molecules than surfactant molecules.

To determine the polarity of the environment surrounding the probe molecules, we compared the CD stretch frequencies of the probes in the micelles to those of the same (or similar) molecules in pure water and pure *n*-hexane. The red horizontal lines in Figure 4 correspond to the CD frequency of hexane-d_{14} (panels A and C) and benzene-d_6 (panels B and D) dissolved in (non-deuterated) liquid *n*-hexane. The solid blue line in Figure 4, panels B and D, represents the CD frequency of benzene-d_6 in water. The dashed blue lines in Figure 4, panels A and C, are estimates of the CD stretch frequency of hexane-d_{14} in water obtained by measuring the difference between the CD peak frequency of 1-hexanol-d_{13} when dissolved in hexane and water. The points in Figure 4 are the CD stretch frequencies of the probes within the micelles. These results reveal that the CD stretch Raman shift of hexane-d_{14} in both the C_9COONa and C_{10}TAB micelles is indistinguishable from the CD frequency of hexane-d_{14} dissolved in *n*-hexane, thus clearly implying that *n*-hexane-d_{14} is solubilized into a region of the micelle that resembles a dry bulk oil phase. This conclusion is consistent with previous NMR studies showing that alkanes are solubilized in the interior of micelles.[44,48,57,58] Similarly, the results in the inset of Figure 4B imply that benzene-d_6 is also solubilized in a dry oil-like environment within C_9COONa micelles, again consistent with some previous studies.[47,57] However, our results do not appear to be consistent with other studies in SDS micelles implying that that benzene is either uniformly distributed throughout the micelle[49,58] or remains at the micelle−water interface.[45] Moreover, the inset of Figure 4D shows, unexpectedly, that the CD stretch frequency of solubilized benzene-d_6 is red-shifted to a greater degree than when it is transferred from water to liquid hexane. Thus, benzene is evidently in an environment that is neither like water nor like hexane, implying a significant interaction between benzene and the surface of the C_{10}TAB surfactants, as suggested by previous studies.[49,58] The anomalous CD frequency shift, as well as the higher rate at which benzene is taken up by C_{10}TAB micelles, suggest the importance of cation−π interactions between benzene and the cationic surfactant headgroup.[49,58] However, previous spectroscopic measurements of benzene−water and benzene−cation clusters indicate that cation−π interactions produce a blue-shift rather than a red-shift in the corresponding aromatic CH stretch frequencies.[59−62] Thus, our observation of an anomalously large red-shift of the CD stretch of benzene-d_6 in C_{10}TAB micelles suggests that benzene may also interact with the bromide (Br^-) counteranions, which are known to red-shift the CH stretch of benzene in aqueous salt solutions.[63] Thus, our results suggest that benzene molecules near the micelle surface interact with both the $-N(CH_3)_3^+$ head groups and Br^- counterions.

Although some previous studies have suggested that non-polar probes may expel water molecules from the micelle interior,[57] we see no evidence of such probe induced drying in our Raman-MCR spectra. More specifically, if there were such probe-induced drying then we would expect to see a significant decrease in the SC OH band area with increasing probe solubilization, which is not evident in the spectra shown in Figure 4.

SUMMARY AND DISCUSSION

Although the structure of micelles has been a topic of longstanding interest,[1−14] previous studies have often reached conflicting conclusions regarding the surface roughness and hydrophobic hydration of micelles.[9] The present Raman-MCR results have addressed these questions by measuring changes in the vibrational spectra of surfactant hydration shells upon micelle formation, and using solubilized hexane and benzene to probe the polarity of the micelle core.

Our findings indicate that surfactant tails remain significantly hydrated, with well over 20% of the surfactant methylene groups remaining in contact with water within the micelle. Moreover, the relative areas of the hydration shell H-bonded and dangling OH bands imply that water molecules within micelles have a lower H-bonding probability than water molecules in the hydrophobic hydration shells of isolated (non-aggregated) surfactants dissolved in water.

Additionally, we have observed a strong chain-length-dependent increase in the average number of hydrophobic hydration shell dangling OH groups (per surfactant). This observation provides compelling evidence that micelles do not have a smooth (nearly spherical) surface, but rather must contain non-polar pores whose surface area increases with increasing surfactant chain length. Although such a surface area increase may in principle be due to either an increase in the number or depth of the non-polar pores (per surfactant), we favor the latter explanation, as it is physically reasonable to expect that longer surfactants will facilitate the formation of deeper pores. Note that the formation of such pores also implies that micelles have a remarkably low surface tension, which does not seem to be consistent with assumptions made in formulating the Gruen model.[34]

Although our results are incompatible with smooth spherical micelle models (including ones in which water only penetrates to the first few methylene groups adjacent to the polar headgroup),[22−25] our findings are generally consistent with models such as that shown in Figure 1D,[35] whose surface contains deep, water-accessible "wedges", as well as with the similar Menger model.[10] In keeping with the structure illustrated in Figure 1D, our dangling OH observations further imply that micelle hydrophobic pores have a depth that increases with surfactant chain length. Moreover, in keeping with Figure 1D and the Menger model, our non-polar probe results confirm that micelles retain a substantially dry hydrophobic core.

One might expect molecular dynamics simulations to provide invaluable information regarding micelle structure and hydration.[24,29,64] However, it is only now beginning to become feasible to perform such simulations on systems that are sufficiently large, with sufficiently long simulation times, to realistically describe fully equilibrated micellar systems. Nevertheless, simulations have already provided important insights. For example, a recent interestingly designed set of simulations suggests that the degree of delocalization of the head groups at the micelle surface can significantly influence the distribution of solubilized molecules.[29] Another large-scale simulation, which formed micelles from a random distribution of surfactants, has

DOI: 10.1021/jacs.5b06655
J. Am. Chem. Soc. 2015, 137, 10809−10815

concluded that the concentration of free monomers may decrease rather than remain constant above CMC.[65] We have recently initiated an effort to perform large-scale fully equilibrated micelle simulations, in collaboration with Prof. Dominik Horinek's group. Preliminary results of those simulations (which will be fully described in a subsequent publication) reveal micelles with highly corrugated surfaces and substantial hydrophobic hydration.

Our conclusion that micelles composed of ionic surfactants do not have a smooth spherical structure implies that the average distance between the ionic head groups is greater than the ∼1 nm separation predicted for an idealized smooth spherical micelles, as indicated by the ∼90 Å^2 (∼0.9 nm^2) area per surfactant shown in Figure 1A. This conclusion is consistent with studies of ionic surfactant stabilized oil nanodroplets whose interfacial surfactant concentration was found to saturate at an area >4 nm^2 per surfactant,[66] implying an average separation >2 nm. Thus, the non-spherical interfacial structure of micelles may be linked to the fact that that the optimal distance between ionic head groups is larger than that in an idealized spherical micelle. It is also noteworthy that oil drops stabilized by non-ionic surfactants have been found to accommodate significantly higher surface densities (with an area per surfactant of <0.5 nm^2),[67,68] and thus non-ionic micelles may prove to have structures quite different from those of ionic micelles.[15,16]

The resemblance of proteins to micelles has played an important role in the early development of biochemistry, as proteins were initially postulated to be colloidal aggregates.[69] This is certainly not such a far-fetched idea, as both proteins and micelles are driven to self-assemble by a delicate balance of non-covalent hydrophobic and hydrophilic interactions. It is also noteworthy that, like micelles, approximately 60% of the water-exposed surface of soluble proteins is composed of non-polar groups.[70] The present results further imply that the structures of micelles and proteins may be even more similar than generally recognized, as neither micelles nor proteins are perfectly spherical, and both are prone to form water-accessible hydrophobic cavities.

■ ASSOCIATED CONTENT

Supporting Information

The Supporting Information is available free of charge on the ACS Publications website at DOI: 10.1021/jacs.5b06655.

Experimental methods, spherical micelle calculations, and additional Raman-MCR results (PDF)

■ AUTHOR INFORMATION

Corresponding Author

*bendor@purdue.edu

Notes

The authors declare no competing financial interest.

■ ACKNOWLEDGMENTS

The authors acknowledge financial support for this work from the National Science Foundation (CHE-1213338). We acknowledge Sylvie Roke for useful discussions and suggestions. Samual Zukowski and Joseph Thomaz are acknowledged for assistance in collecting experimental results of relevance to this work.

■ REFERENCES

(1) Murray, R. C.; Hartley, G. S. *Trans. Faraday Soc.* **1935**, *31*, 183.
(2) Dill, K. A.; Flory, P. J. *Proc. Natl. Acad. Sci. U. S. A.* **1981**, *78*, 676.
(3) Stigter, D. *J. Phys. Chem.* **1974**, *78*, 2480.
(4) Gruen, D. W. R. *J. Colloid Interface Sci.* **1981**, *84*, 281.
(5) Gruen, D. W. R. *Prog. Colloid Polym. Sci.* **1985**, *70*, 6.
(6) Israelachvili, J. N. *Intermolecular and Surface Forces*, 3rd ed.; Academic Press: San Diego, 2011.
(7) Muller, N.; Birkhahn, R. H. *J. Phys. Chem.* **1967**, *71*, 957.
(8) Svens, B.; Rosenholm, B. *J. Colloid Interface Sci.* **1973**, *44*, 495.
(9) Menger, F. M.; Shi, L. *J. Am. Chem. Soc.* **2006**, *128*, 9338.
(10) Menger, F. M.; Jerkunica, J. M.; Johnston, J. C. *J. Am. Chem. Soc.* **1978**, *100*, 4676.
(11) Menger, F. M.; Doll, D. W. *J. Am. Chem. Soc.* **1984**, *106*, 1109.
(12) Fromherz, P. *Ber. Bunsen-Ges.* **1981**, *85*, 891.
(13) Friman, R.; Rosenholm, J. B. *Colloid Polym. Sci.* **1982**, *260*, 545.
(14) Romsted, L. S. *Langmuir* **2007**, *23*, 414.
(15) Garde, S.; Yang, L.; Dordick, J. S.; Paulaitis, M. E. *Mol. Phys.* **2002**, *100*, 2299.
(16) Maibaum, L.; Dinner, A. R.; Chandler, D. *J. Phys. Chem. B* **2004**, *108*, 6778.
(17) Perera, P.; Wyche, M.; Loethen, Y.; Ben-Amotz, D. *J. Am. Chem. Soc.* **2008**, *130*, 4576.
(18) Davis, J. G.; Gierszal, K. P.; Wang, P.; Ben-Amotz, D. *Nature* **2012**, *491*, 582.
(19) Davis, J. G.; Rankin, B. M.; Gierszal, K. P.; Ben-Amotz, D. *Nat. Chem.* **2013**, *5*, 796.
(20) Davis, J. G.; Zukowski, S. R.; Rankin, B. M.; Ben-Amotz, D. *J. Phys. Chem. B* **2015**, *119*, 9417.
(21) Menger, F. M.; Chow, J. F. *J. Am. Chem. Soc.* **1983**, *105*, 5501.
(22) Berr, S.; Jones, R. R. M.; Johnson, J. S. *J. Phys. Chem.* **1992**, *96*, 5611.
(23) Berr, S. S.; Caponetti, E.; Johnson, J. S.; Jones, R. R. M.; Magid, L. J. *J. Phys. Chem.* **1986**, *90*, 5766.
(24) Hargreaves, R.; Bowron, D. T.; Edler, K. *J. Am. Chem. Soc.* **2011**, *133*, 16524.
(25) Bales, B. L.; Zana, R. *J. Phys. Chem. B* **2002**, *106*, 1926.
(26) Boecker, J.; Brickmann, J.; Bopp, P. *J. Phys. Chem.* **1994**, *98*, 712.
(27) Kuhn, H.; Breitzke, B.; Rehage, H. *Colloid Polym. Sci.* **1998**, *276*, 824.
(28) Shelley, J.; Watanabe, K.; Klein, M. L. *Electrochim. Acta* **1991**, *36*, 1723.
(29) Mizuguchi, T.; Ishizuka, R.; Matubayasi, N. *Chem. Phys. Lett.* **2015**, *624*, 19.
(30) McBain, J. W.; Kawakami, Y.; Lucas, H. P. *J. Am. Chem. Soc.* **1933**, *55*, 2762.
(31) McBain, J. W.; Johnson, K. E. *J. Am. Chem. Soc.* **1944**, *66*, 9.
(32) Vetter, R. J. *J. Phys. Colloid Chem.* **1947**, *51*, 262.
(33) Courchene, W. L. *J. Phys. Chem.* **1964**, *68*, 1870.
(34) Gruen, D. W. R. *J. Phys. Chem.* **1985**, *89*, 153.
(35) Reprinted with permission from Elsevier from the following: Svens, B.; Rosenholm, B. *J. Colloid Interface Sci.* **1973**, 495−504.
(36) Gierszal, K. P.; Davis, J. G.; Hands, M. D.; Wilcox, D. S.; Slipchenko, L. V.; Ben-Amotz, D. *J. Phys. Chem. Lett.* **2011**, *2*, 2930.
(37) Rankin, B. M.; Ben-Amotz, D.; van der Post, S. T.; Bakker, H. J. *J. Phys. Chem. Lett.* **2015**, *6*, 688.
(38) Lawton, W. H.; Sylvestr, E. A. *Technometrics* **1971**, *13*, 617.
(39) Tomlinson-Phillips, J.; Davis, J.; Ben-Amotz, D.; Spangberg, D.; Pejov, L.; Hermansson, K. *J. Phys. Chem. A* **2011**, *115*, 6177.
(40) Perera, P. N.; Browder, B.; Ben-Amotz, D. *J. Phys. Chem. B* **2009**, *113*, 1805.
(41) Mukerjee, P.; Mysels, K. J. *Critical Micelle Concentrations of Aqueous Surfactant Systems*; National Bureau of Standards: Washington, DC, 1971; Vol. NSRDS-NBS *36*, pp 1−222.
(42) Scheu, R.; Chen, Y.; de Aguiar, H. B.; Rankin, B. M.; Ben-Amotz, D.; Roke, S. *J. Am. Chem. Soc.* **2014**, *136*, 2040.
(43) Scheu, R.; Rankin, B. M.; Chen, Y. X.; Jena, K. C.; Ben-Amotz, D.; Roke, S. *Angew. Chem., Int. Ed.* **2014**, *53*, 9560.

DOI: 10.1021/jacs.5b06655
J. Am. Chem. Soc. 2015, 137, 10809−10815

(44) Henriksson, U.; Klason, T.; Ödberg, L.; Eriksson, J. C. *Chem. Phys. Lett.* **1977**, *52*, 554.
(45) Mukerjee, P.; Cardinal, J. R. *J. Phys. Chem.* **1978**, *82*, 1620.
(46) Menger, F. M.; Boyer, B. J. *J. Am. Chem. Soc.* **1980**, *102*, 5936.
(47) Jobe, D. J.; Reinsborough, V. C.; White, P. J. *Can. J. Chem.* **1982**, *60*, 279.
(48) Tornblom, M.; Henriksson, U. *J. Phys. Chem. B* **1997**, *101*, 6028.
(49) Hawrylak, B. E.; Marangoni, D. G. *Can. J. Chem.-Rev. Can. Chim.* **1999**, *77*, 1241.
(50) Menger, F. M.; Yoshinaga, H.; Venkatasubban, K. S.; Das, A. R. *J. Org. Chem.* **1981**, *46*, 415.
(51) Muller, N.; Simsohn, H. *J. Phys. Chem.* **1971**, *75*, 942.
(52) Vitha, M. F. In *Interfaces and Interphases in Analytical Chemistry*; Helburn, R., Vitha, M. F., Eds.; American Chemical Society: Washington, DC, 2011; Vol. *1062*, p 19.
(53) Nagarajan, R.; Chaiko, M. A.; Ruckenstein, E. *J. Phys. Chem.* **1984**, *88*, 2916.
(54) McGrath, J. A.; Parkerton, T. E.; Hellweger, F. L.; Di Toro, D. M. *Environ. Toxicol. Chem.* **2005**, *24*, 2382.
(55) Rodriguez-Pulido, A.; Casado, A.; Munoz-Ubeda, M.; Junquera, E.; Aicart, E. *Langmuir* **2010**, *26*, 9378.
(56) Chakraborty, I.; Moulik, S. P. *J. Phys. Chem. B* **2007**, *111*, 3658.
(57) Eriksson, J. C.; Gillberg, G. *Acta Chem. Scand.* **1966**, *20*, 2019.
(58) Wasylishen, R. E.; Kwak, J. C. T.; Gao, Z. S.; Verpoorte, E.; Macdonald, J. B.; Dickson, R. M. *Can. J. Chem.* **1991**, *69*, 822.
(59) Bandyopadhyay, B.; Cheng, T. C.; Wheeler, S. E.; Duncan, M. A. *J. Phys. Chem. A* **2012**, *116*, 7065.
(60) Gruenloh, C. J.; Carney, J. R.; Arrington, C. A.; Zwier, T. S.; Fredericks, S. Y.; Jordan, K. D. *Science* **1997**, *276*, 1678.
(61) Jaeger, T. D.; Pillai, E. D.; Duncan, M. A. *J. Phys. Chem. A* **2004**, *108*, 6605.
(62) Jaeger, J. B.; Pillai, E. D.; Jaeger, T. D.; Duncan, M. A. *J. Phys. Chem. A* **2005**, *109*, 2801.
(63) Vincent, J. C.; Matt, S. M.; Rankin, B. M.; D'Auria, R.; Freites, J. A.; Ben-Amotz, D.; Tobias, D. J. *Chem. Phys. Lett.* **2015**, *638*, 1.
(64) Lima, F. S.; Chaimovich, H.; Cuccovia, I. M.; Horinek, D. *Langmuir* **2014**, *30*, 1239.
(65) Sanders, S. A.; Sammalkorpi, M.; Panagiotopoulos, A. Z. *J. Phys. Chem. B* **2012**, *116*, 2430.
(66) de Aguiar, H. B.; de Beer, A. G.; Strader, M. L.; Roke, S. *J. Am. Chem. Soc.* **2010**, *132*, 2122.
(67) Chen, Y.; Jena, K. C.; Lütgebaucks, C.; Okur, H. I.; Roke, S. *Nano Lett.* **2015**, DOI: 10.1021/acs.nanolett.5b02143.
(68) Chen, Y.; Jena, K. C.; Roke, S. *J. Phys. Chem. C* **2015**, *119*, 17725.
(69) Tanford, C. *The Hydrophobic Effect*, 2nd ed.; Wiley-Interscience: New York, 1980.
(70) Miller, S.; Janin, J.; Lesk, A. M.; Chothia, C. *J. Mol. Biol.* **1987**, *196*, 641.

DOI: 10.1021/jacs.5b06655
J. Am. Chem. Soc. 2015, 137, 10809−10815